Generalized hydrodynamics for a Poiseuille flow: Theory and simulations

Dino Risso*
Departamento de Física, Facultad de Ciencias, Universidad del Bío-Bío, Casilla 5C, Concepción, Chile

Patricio Cordero†
Departamento de Física, Facultad de Ciencias Físicas y Matemáticas, Universidad de Chile, Casilla 487, Santiago 3, Chile
(Received 29 January 1998)

From the complete Boltzmann's equation we obtain general hydrodynamic equations for the laminar stationary Poiseuille flow driven by an acceleration of gravity g. This theoretical framework implies highly nonlinear transport equations. The hydrodynamic equations are perturbatively solved up to sixth order using a small adimensional parameter $\mathcal{F}$ proportional to g. The predictions are compared with our own simulational results obtaining very good agreement. A second and small adimensional parameter that naturally enters the formalism is a Knudsen number Kn proportional to the ratio between the mean free path and the width of the Poiseuille channel and it serves to understand the role of the finite size effects. It will be seen in particular that there is a heat flux with a normal component q_y and a heat flux q_x parallel to the isotherms and that their ratio is inversely proportional to the Reynolds number: $q_x/q_y \sim \mathcal{F}/\mathrm{Kn} \sim 1/\mathrm{Re}$. [S1063-651X(98)08707-8]

PACS number(s): 05.20.Dd, 47.50.+d, 51.10.+y

I. INTRODUCTION

This paper presents a Poiseuille flow that shows a behavior beyond the scope of standard hydrodynamics. The Poiseuille flow is a classical example to study by means of the Navier-Stokes equations [1–3]. Perhaps the first molecular-dynamic simulation of this flow is the one reported in [4]. Usually the Poiseuille flow is understood to be driven by an externally imposed pressure gradient, but it is trivially equivalent to applying a gravitational force mg over each particle [5,6]. For small velocities (small Reynolds or Mach number) the flow is known to be laminar and stationary and the velocity profile is parabolic. There is, however, a critical Reynolds number above which an unstable (turbulent) regime starts [2]. In [7] the authors studied a small system of Lennard-Jones particles observing that in spite of the size of the system it has a good hydrodynamic behavior.

In this paper we present analytic and simulational results regarding the Poiseuille flow of a two-dimensional system of hard particles in a regime deeply inside the stable zone. The corresponding theoretical results in the 3D case are presented in the final section. An interesting feature of our system of hard particles is that it presents important thermal and compressibility effects. Hence this numerical system represents a challenge to the theory of hydrodynamics since its transport coefficients depend on position. A relatively recent and quite thorough numerical analysis of the 2D Poiseuille flow is found in [8].

It will be shown that our simulational observations fall beyond standard hydrodynamics: the transport laws are nonlinear and effects related to the small ratio of the mean free path and the width of the channel are observable. We present a hydrodynamics derived directly from Boltzmann's equation, which includes, besides the balance of mass, momentum, and energy, extra balance equations that take the place of the usual constitutive equations. These extra equations are derived from Boltzmann's equation using a moment expansion of the distribution. The whole picture is valid in the Boltzmann-Grad limit of low density and small, but finite, mean free path. We call such dynamics *Boltzmann-Grad gas-dynamics* since Grad pioneered moment expansions in the present context [9]. Besides Grad's already cited articles, we have made presentations and applications of Boltzmann-Grad gas-dynamics in [10–12]. It has to be underlined that in the present framework no constitutive transport equations are assumed. Instead, the derived gas-dynamics contains equations and they replace Newton's and Fourier's laws.

In [2] it has been shown that for a two-dimensional incompressible Poiseuille flow in an infinitely long channel the predicted critical Reynolds number is $\mathrm{Re}_c = 5772$ corresponding to long wave excitations [6]. But when the aspect ratio $\lambda =$ width/length is finite, the value of Re_c increases since these long wave excitations cannot exist. In [6] the authors have studied the stability curve λ versus Re_c that stems from a linear stability analysis. In particular from their results it is seen that for aspect ratio $\lambda = 1$ or $\lambda = 4$—which we use—$\mathrm{Re}_c \geqslant 10^6$. In view of this we can state that the numerical experiments that we present in the present paper are deeply in the stable region ($\mathrm{Re} < 100$).

One could say that the results in this work should be expected because we know that Boltzmann's equation has to describe correctly a system such as the one we deal with. The point is, however, that it is not obvious how to extract the information from Boltzmann's equation. Many applications of Boltzmann's equations use the Chapman-Enskog method to extract the information concealed in this very complex kinetic equation [13] or, if not, they use the approximate Bhatnagar-Gross-Krook (BKG) equation; in the context of the Poiseuille flow see [5,14–16]. Up to second order the Chapman-Enskog method is quite involved and leads to linear constitutive equations, therefore it cannot describe what we do here.

*Electronic address: drisso@enskog.dfi.uchile.cl
†Electronic address: pcordero@cec.uchile.cl

As already said, we use Grad's moment expansion method [9], which has already been proved to produce quite nontrivial nonlinear constitutive equations that describe extraordinarily well the observations obtained from molecular-dynamic simulations [10–12]. We particularly underline that in [10] we were able to find a close analytic solution of the gas-dynamic equations for the case of a planar Couette flow, and they describe extremely well the simulational observations. Interesting fits to some of the results given in [10] using a modified Boltzmann equation are given in [17].

In Sec. II we present the gas-dynamic equations for the bidimensional laminar Poiseuille flow, the boundary and integral conditions, and a low-order nontrivial perturbative solution. In Sec. III after explaining the molecular-dynamic simulations that were made, a comparison between the theory of Sec. II and the simulational results is made. Section IV presents the gas-dynamic equations and a low-order solution of the 3D case. The Appendix contains the perturbative solution up to sixth order for the bidimensional case.

II. POISEUILLE LAMINAR FLOW GAS-DYNAMICS

In this section we present the hydrodynamic equations for a laminar 2D Poiseuille flow along a channel with walls parallel to the X axis placed at $y=\pm L_y/2$. The fluid moves under the effect of a gravitational acceleration $\vec{g}=g\hat{x}$, it has N_x particles per unit length along the channel and the walls are kept at a fixed temperature T_0.

A. Gas-dynamic equations

From Boltzmann's equation it is straightforward to derive balance equations for mass, momentum, and energy. The balance equations stemming from higher moments of the distribution function are not so simple to derive since they are not associated to microscopically conserved quantities. They are obtained using some truncation assumptions, as Grad did. In this way balance equations associated to the pressure tensor, P_{ij}, and the heat flux vector, q_k, follow and they are *dynamical equations* that totally replace the usually linear and static constitutive transport equations. We have reconstructed Grad's derivation of these higher balance equations for the case of a dilute 2D gas of hard disks and they are found in [10,11]. Once the whole set of balance equations is specialized to the Poiseuille flow, the problem is reduced to a set of five coupled nonlinear differential equations, some algebraic equations, a boundary condition, some symmetry properties, and an integral condition. We remark that Grad's solution cannot be expected to be valid near the boundaries where the interaction with the walls plays an important distorting role particularly at low densities because the formalism does not take into consideration wall effects.

Before we write down the basic hydrodynamic equations for the laminar Poiseuille flow, we define adimensional fields that, instead of being functions of the transversal coordinate y, are defined as functions of $\xi\equiv y/L_y$,

$$T^*(\xi)=\frac{T(y)}{T_0},$$

$$P^*_{ij}(\xi)=\frac{P_{ij}(y)}{p_0}, \tag{1}$$

$$q^*_k(\xi)=\frac{q_k(y)}{q_0},$$

where

$$p_0\equiv\frac{N_xT_0}{L_y} \quad \text{and} \quad q_0\equiv\frac{1}{2}p_0\sqrt{\frac{T_0}{m}}=\frac{2\rho_AT_0^{3/2}}{\pi\sqrt{m}\sigma^2}. \tag{2}$$

The temperature field T is expressed in energy units such that Boltzmann's constant is $k_B=1$. The particles have mass m and diameter σ; $\rho_A=(\pi\sigma^2/4)(N_x/L_y)$ is the global area density and N_x is the number of particles per unit length. It is convenient to define an adimensional field γ that measures the intensity of the shear rate

$$\gamma=\frac{1}{2\sigma p}\sqrt{\frac{mT}{\pi}}\frac{dv_x}{dy}, \tag{3}$$

where p is the hydrostatic local pressure.

When the equations are written in terms of these quantities some parameters emerge naturally. They are

$$\mathrm{Kn}=\frac{2}{\sqrt{\pi}\sigma N_x}\propto\frac{l}{L_y} \quad \text{and} \quad \mathcal{F}=\frac{mgL_y}{T_0}\frac{1}{\mathrm{Kn}}. \tag{4}$$

The parameter $\mathcal{F}$ serves to control the intensity of the velocity field. Kn is proportional to the ratio between the mean free path $l=\pi\sigma/(8\sqrt{2}\rho_A)$ and the transversal linear size of the box, hence it is a Knudsen number and it serves as a good descriptor of finite size effects. The complete picture is worked out under the assumption that Kn is small, otherwise we would be dealing with a Knudsen gas.

The mass balance equation is satisfied identically. The rest of the balance equations are the following. The momentum balance yields

$$P^*_{yy}=\text{const}, \tag{5}$$

$$\mathrm{Kn}\frac{dP^*_{xy}}{d\xi}=\mathcal{F}\mathrm{Kn}^2\frac{p^*}{T^*}. \tag{6}$$

The energy balance becomes

$$\frac{\mathrm{Kn}}{8}\frac{\sqrt{T^*}}{p^*}\frac{dq^*_y}{d\xi}=-\gamma P^*_{xy}. \tag{7}$$

The equations associated to the balance of the P_{ij} give

$$p^*=P^*_{yy}-\frac{3}{2}\gamma P^*_{xy}, \tag{8}$$

$$\frac{\mathrm{Kn}}{16}\frac{\sqrt{T^*}}{p^*}\frac{dq^*_x}{d\xi}=-\gamma P^*_{yy}-P^*_{xy}. \tag{9}$$

And finally the q_k balance equations are

$$-3\frac{\mathrm{Kn}\sqrt{T^*}}{p^*}P^*_{xy}\frac{dT^*}{d\xi}=q^*_x+3\gamma q^*_y+\frac{\mathcal{F}\mathrm{Kn}^2}{p^*}\sqrt{T^*}P^*_{yy}, \tag{10}$$

$$\frac{\mathrm{Kn}\sqrt{T^*}}{p^*}\left(2P^*_{yy}\frac{dT^*}{d\xi}-\frac{3}{2}\frac{d}{d\xi}\{\gamma P^*_{xy}T^*\}\right)$$

$$=q^*_y+\gamma q^*_x+\frac{\mathcal{F}\mathrm{Kn}^2\sqrt{T^*}}{p^*}P^*_{xy}. \tag{11}$$

Equations (6), (7), (9), (10), and (11) are five coupled differential equations for the five fields P^*_{xy}, q^*_y, q^*_x, T^*, and γ. To completely solve the hydrodynamic problem it is necessary to find also the uniform field P^*_{yy}. The hydrostatic pressure is determined from Eq. (8) and $P^*_{xx}=2p^*-P^*_{yy}$.

In these equations the derivatives appear multiplied by Kn suggesting that it would be more natural to use as adimensional transversal coordinate the quantity $\zeta\equiv\xi/\mathrm{Kn}$, but then the integral condition described below introduces Kn separately since Eq. (14) would be $\int p^*/T^*d\zeta=1/\mathrm{Kn}$.

Equations (9) and (11) are rather complex equations that take the place of the usual laws of viscous flow and of transversal heat transport, respectively. In our case they have been derived rather than introduced as assumptions.

B. Boundary and integral conditions

The temperature is fixed at the walls so that

$$T^*\left(\pm\frac{1}{2}\right)=1. \tag{12}$$

From the differential equations and the boundary condition (12) it follows that the hydrodynamic fields of the present problem have two parities, one with respect to changing the sign of $\mathcal{F}$ and the other one with respect to inverting ξ. These parities are given in expression (13),

	$\mathcal{F}\to-\mathcal{F}$	$\xi\to-\xi$
γ	$-$	$-$
T^*	$+$	$+$
q^*_x	$-$	$+$
q^*_y	$+$	$-$
P^*_{xy}	$-$	$-$
P^*_{yy}	$+$	$+$

(13)

The explicit use of these parities plus the boundary condition mentioned above is enough to determine a unique solution of the differential equations except that P^*_{yy} is not yet determined.

To obtain P^*_{yy} it is necessary to use the ideal gas equation of state derived in the Boltzmann-Grad limit: $p=nT$, where $n(y)$ is the number density. Since $\int n(y)dy$ integrated over the width of the channel gives the density per unit length, N_x, then

$$\int_{-1/2}^{1/2}\frac{p^*(\xi)}{T^*(\xi)}d\xi=1. \tag{14}$$

From Eq. (6) it is seen that $P^*_{xy}(\xi)$ has to satisfy

$$P^*_{xy}\left(\pm\frac{1}{2}\right)=\pm\frac{1}{2}\mathcal{F}\mathrm{Kn}, \tag{15}$$

since $P^*_{xy}(\xi)$ is antisymmetric in ξ, but this is not an independent condition.

C. Perturbative solution

The acceleration of gravity is the agent that takes the system out of equilibrium. It is natural then to take g, or rather $\mathcal{F}$, as the small parameter to iteratively find a solution. Assuming analyticity at $\mathcal{F}=0$ the set of differential equations and the boundary condition can easily be solved consistently order by order.

At the trivial order $\mathcal{F}=0$ all fields vanish except $T^*=1$ and $P^*_{yy}=1$.

It is easy to check that the second order solution is

$$P^*_{xy}=\xi\mathrm{Kn}\mathcal{F},\quad \gamma=-\xi\mathrm{Kn}\mathcal{F},$$

$$P^*_{yy}=1+\left[\frac{1}{60}-\frac{\mathrm{Kn}^2}{4}\right]\mathcal{F}^2,$$

$$T^*(\xi)=1+\left[\frac{1}{48}-\frac{\xi^4}{3}+\left(\frac{3\xi^2}{4}-\frac{3}{16}\right)\mathrm{Kn}^2\right]\mathcal{F}^2, \tag{16}$$

$$q^*_x=-\mathcal{F}\mathrm{Kn}^2,\quad q^*_y=\frac{8}{3}\xi^3\mathcal{F}^2\mathrm{Kn},$$

from where it follows that

$$p^*=1+\left[\frac{1}{60}+\left(\frac{3}{2}\xi^2-\frac{1}{4}\right)\mathrm{Kn}^2\right]\mathcal{F}^2. \tag{17}$$

The pressure is not uniform but its nonuniformity is quite small since it is proportional to $\mathrm{Kn}^2\mathcal{F}^2$. The temperature profile is not parabolic and its nonuniformity is dominated by a ξ^4 term. At this order one can already see a quadratic correction to the ξ^4 profile, which is there because the Knudsen number Kn is finite. This correction corresponds to the one in Eq. (21) of [18]. See also [19] and [12].

Newton's law of viscous flow in the present adimensional formulation is $P^*_{xy}=-p^*\gamma$ and up to second order it is satisfied but at higher orders it is known that this is not the case as seen, for example, in [12]. Fourier's law in adimensional form is $q^*_y=-2\mathrm{Kn}(dT^*/d\xi)$, which is not quite true at the present order. The small difference, to this order, is $3\mathrm{Kn}^3\xi$. One should perhaps be surprised that there is a heat flux q_x parallel to the isotherms; it is small but it is there. This nonstandard flux (parallel to the isotherms) has already been mentioned in the literature and derived from Boltzmann's equation, as, for example, in [10,12,14,15].

Integrating the expression for γ and using definition (3), yields the usual parabolic velocity profile

$$v^*_x\equiv\sqrt{\frac{m}{T_0}}v_x=2\mathcal{F}\left(\frac{1}{4}-\xi^2\right). \tag{18}$$

Hence the hydrodynamic velocity at the center of the channel at low order, from Eq. (18), is proportional to $\mathcal{F}$,

$$v^*_{\text{center}}=\frac{\mathcal{F}}{2}, \tag{19}$$

as it has already been mentioned.

In Appendix A we give the solution of our system up to sixth order in $\mathcal{F}$ while in the next section we show how well our solution fits with our observations. It can be checked that the fourth order is enough to explain the fits presented in the next section. In fact, the sixth-order corrections are negligible in the cases we have considered.

III. SIMULATIONAL CONDITIONS AND SIMULATION-THEORY COMPARISON

A. Generalities

Our main simulations consider a system of $N=7056$ particles in a channel of length $L_x=372.22\sigma$ and width $L_y=1488.86\sigma$. We have also made simulations with a larger system of $N=28224$ particles, in a channel with $L_x=L_y=1488.9\sigma$. This implies, in both cases, that the global area density is $\rho_A=0.01$. With this choice the nonideal corrections to the equation of state are less than 2%. The size of the system is large enough that the ratio between the *mean free path*, $l=\pi\sigma/(8\sqrt{2}\rho_A)$, and the width L_y of the channel is about 0.019.

Units are chosen so that the mass of each particle is $m=1$, their diameter is $\sigma=1$, and time units are such that the externally imposed temperature T_0 expressed in energy units ($k_B=1$) is fixed to be $T_0=1$. The collisions among particles are perfectly elastic. The vertical walls (along the Y direction) are treated as periodic boundaries, and the collisions with the hard horizontal walls (along the X direction) are such that they impose $T_0=1.0$ at the walls as well as a null velocity. In both cases ($N=28224$ and $N=7056$) the external acceleration has been chosen $g=0.124(T_0/mL_y)=0.000\,083$, which corresponds to $\mathcal{F}\approx 2.07$.

For finite systems there is a wall temperature jump that cannot be neglected, implying that the limit $T(y\rightarrow\text{wall})$ does not give exactly the value externally imposed. As it will be seen below, the effective values for T_0 are $T_0=1.10$ in the case $N=28\,224$ and $T_0=1.58$ for $N=7056$, implying effective values $\mathcal{F}=1.89$ and $\mathcal{F}=1.31$, respectively. The value of the Reynolds number in our simulations is $\text{Re}\approx 67$ for $N=7056$ and $\text{Re}\approx 42$ for $N=28\,224$.

In every simulation the system was relaxed for about three thermal diffusion times, t_{diff}, before local time averages of the main moments of the distribution $(n,\vec{v},T,p_{ij},\vec{q})$ were taken. The temporal averages were taken for as long as 30 t_{diff} in the case of $N=7056$, and 46.5 t_{diff} in the case of $N=28\,224$. In one t_{diff} each particle suffers about 500 particle collisions when $N=7056$ and about 1000 particle collisions when $N=28\,224$.

To measure the hydrodynamic behavior of the system, the box is divided in $M_x\times M_y$ rectangular cells. Time averages of the first moments of the distribution are made in each cell. For the system with $N=28\,224$ particles the choice was $M_x=M_y=28$, which corresponds to about 36 disks per cell, while in the case with $N=7056$ the choice was $M_x=21$, $M_y=84$, or about 4.0 disks per cell.

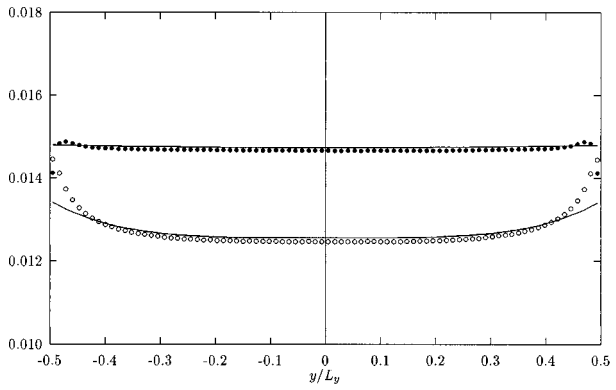

FIG. 1. Density and pressure profile for the $N=7056$ system. The circles give the simulational results (see text) and the solid lines correspond to the theoretical predictions up to sixth order. The solid and open circles represent the pressure and density, respectively.

In the case $N=7056$, the statistics was improved making 21 independent runs using equivalent macroscopic initial conditions, which differed only microscopically. The results discussed below correspond to the ensemble of these simulations.

Taking advantage of the translation invariance in the X direction, it was natural to take horizontal averages of the observed cell results getting in this way smooth vertical profiles for the observed hydrodynamic fields.

B. Theory versus simulations

Most quantities show boundary effects. The temperature field shows isotherms parallel to the flow but—as predicted by Eqs. (10) and (11)—the heat flux is not orthogonal to them. The heat flux parallel to the flow (and to the isotherms) will be discussed further along and it can be seen in Fig. 5. In a wide central part it points against the flow while nearer to the walls its sign changes as predicted.

The equation of state is well satisfied across the fluid, including the regions near the walls. Observed discrepancies with the ideal gas equation were always below 2% and if Henderson's equation of state [20] is used the discrepancies are below 0.1%.

P_{yy} should be uniform, see Eq. (5), and this is what we in fact observe. From the horizontal average of the observed P_{yy}, the value at each y is obtained with errors of less than 0.4%. An additional vertical average over the previous profile produces a variance of about 10^{-8}%. In this sense it can be stated that P_{yy} is independent of y as our equations predict.

As a consequence of finite size the temperature has a discontinuity at the walls. We use this fact to consider T_0 as a *parameter* to be determined. With this aim we equate the measured P_{yy} with the theoretical $P_{yy}=p_0P^*_{yy}$, written up to sixth order, to obtain an effective T_0. In this way we determine an effective value: $T_0=1.10$ for the $N=7056$ system, and $T_0=1.58$ for $N=28\,224$. The other theoretical profiles obtained using these values for T_0 are then directly compared with the simulational results finding that usually they almost coincide. Details follow.

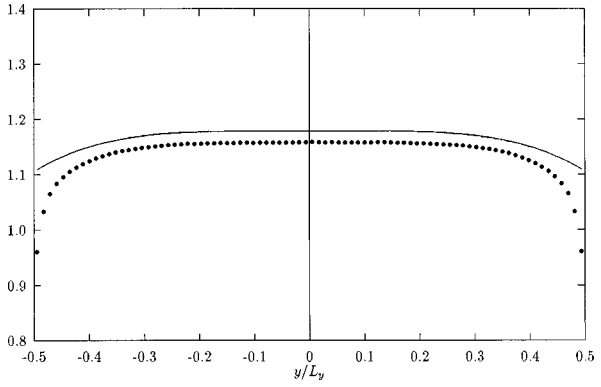

FIG. 2. Temperature profile T/T_0 for the $N=7056$ system. The circles give the simulational results and the solid line corresponds to the theoretical prediction up to sixth order. The discrepancy in the central region is of about 1.7%.

1. Thermodynamic fields

The pressure that we predict is in excellent agreement with what we observe (solid circles in Fig. 1), the discrepancies being less than 0.5%. Only in a narrow region near the walls are there deviations that reach 6%.

The density profile (open circles in Fig. 1) shows important boundary effects. Near the walls theory underestimates the density by about 7%. Since the global density is fixed, this implies that the mean density in the central region is slightly smaller (about 0.48%) than what is predicted by the theory.

On the other hand, Henderson's equation of state [20] is extremely well satisfied. For this reason the theoretical prediction of the temperature via the equation of state of an ideal gas $T=p/n$ underestimates the observed temperature by about 2%, as can be appreciated in Fig. 2. The discrepancy in the central region is of about 1.7%.

2. Shear and velocity fields

Figure 3 compares the differences $\Delta\gamma=\gamma_{\text{theo.}}-\gamma_{\text{sim.}}$ between the theoretical predictions (first and third order) and the simulational values for the γ profile. It can be seen that the third-order correction values give a better description of

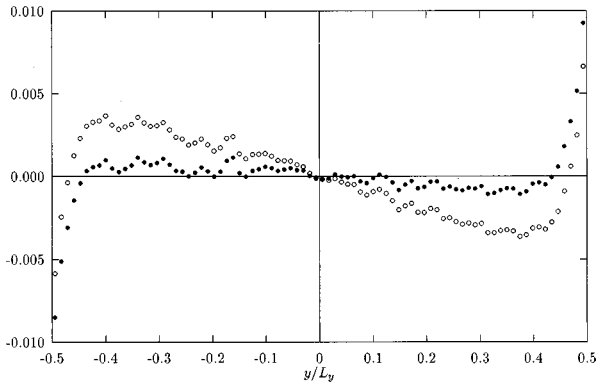

FIG. 3. The plot shows the difference $\Delta\gamma=\gamma_{\text{theo.}}-\gamma_{\text{sim.}}$ between the predicted and the observed values of the shear rate profile for the $N=7056$ system. The open (solid) circles show the difference considering $\gamma_{\text{theo.}}$ evaluated up to first (third) order. Up to third order these differences, away from the walls, are of about 2%.

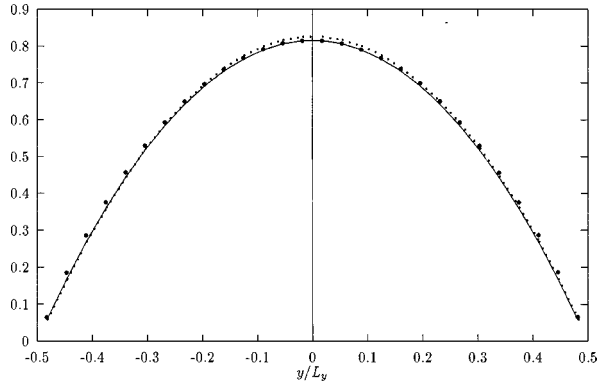

FIG. 4. The v_x velocity profile, scaled with the factor $\sqrt{T_0/m}$, for the $N=28\,224$ system. The circles give the simulational results, the dotted line gives the first-order correction. The velocity profile up to third and fifth order are indistinguishable and correspond to the solid line.

the observations (the discrepancy in this case being about 2% except very near the boundary region).

Plotting the observed values of P_{xy} and $-p\gamma$ produces coincident points, namely, the deviations from Newton's law cannot be observed. The reason can be understood because P_{xy} and $-p\gamma$ at first order coincide [they are $O(\text{Kn}\mathcal{F})$] while $P_{xy}+p\gamma$ is $O(\text{Kn}^3\mathcal{F}^3)$. The difference between these two observables is smaller than the precision with which we observe these quantities.

Figure 4 has the velocity profile v_x in the case of $N=28\,224$ particles. The velocity at the center of the channel is slightly overestimated by the first-order correction but at third order there is a better agreement.

3. The heat currents q_x and q_y

Figure 5 refers to the heat flux (q_x,q_y). The solid and open circles represent the observed values of q_x and q_y, respectively.

q_x: the horizontal dotted line is the first order prediction given in Eq. (16); the solid line gives q_x up to fifth order. We do not show q_x up to third order because it almost coincides with the fifth-order profile. The first order gives a uniform negative value that describes well the profile in the central part. To take into account the observations nearer to the

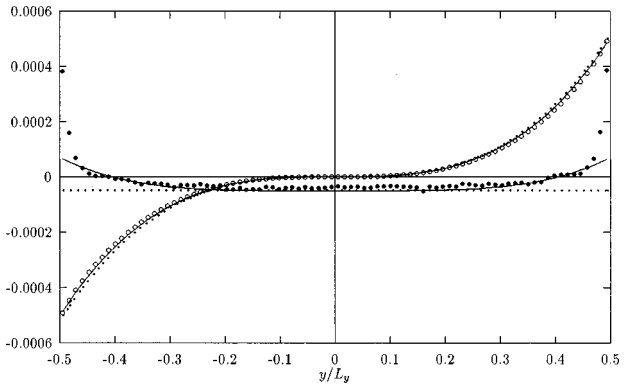

FIG. 5. The heat flux (q_x,q_y), scaled with the factor $T_0\sqrt{T_0/m}$, for the $N=7056$ system. The solid and open circles represent the observed values of q_x and q_y, respectively. See text.

walls at least third-order corrections must be considered.

q_y: the dotted and solid lines give the second- and fourth-order predictions, respectively. For the considered values of $\mathcal{F}$ and Kn the lowest (second) order is enough to reproduce the observed values of q_y (modified Fourier's law) [12]; higher orders are quite negligible. The agreement with the predicted values is excellent.

IV. THREE-DIMENSIONAL GAS-DYNAMIC EQUATIONS

Even though the present paper is centered in a two-dimensional system, many readers may be interested in the corresponding three-dimensional version of the same results. Hence, in this section we give the gas-dynamic equations for a Poiseuille planar stationary flow of hard spheres of mass m and diameter σ between two walls parallel to the X-Y plane at $z=-L_z/2$ and $z=L_z/2$, respectively. The transversal coordinate is z and the system is subjected to $\vec{g}=[g,0,0]$. The walls are kept at a fixed temperature T_0. It is easy to see that $q_y=0$ and $P_{xy}=P_{yz}=0$. The adimensional shear rate γ is defined as

$$\gamma=\frac{5}{16}\frac{1}{\sigma^2 p}\sqrt{\frac{mT}{\pi}}\frac{dv_x}{dz}. \tag{20}$$

The number density $n(z)$ is only a function of z and $\int n(z)dz=N_{xy}$, where N_{xy} is the number of particles per unit surface.

To dimensionalize we use a coordinate ξ such that $z=\xi L_z$ and introduce the adimensional numbers

$$\mathrm{Kn}=\frac{1}{\sqrt{2\pi}\sigma^2 N_{xy}},\quad \mathcal{F}=\frac{mgL_z}{T_0}\frac{1}{\mathrm{Kn}}. \tag{21}$$

Further we use $p_0=T_0N_{xy}/L_z$ and $q_0=p_0\sqrt{T_0/(2m)}$ to define adimensional fields T^*, P^*_{ij}, and q^*_k as in the bidimensional case. The gas-dynamic equations are five differential equations for the nontrivial fields T^*, γ, P^*_{xz}, q^*_z, q^*_x. The uniform field P^*_{zz} is obtained from the integral condition given below. The differential equations are

$$\mathrm{Kn}\frac{dP^*_{xz}}{d\xi}=\mathrm{Kn}^2\mathcal{F}\frac{p^*}{T^*}, \tag{22}$$

$$\frac{\mathrm{Kn}}{8}\frac{\sqrt{T^*}}{p^*}\frac{dq^*_x}{d\xi}=-\gamma P^*_{zz}-P^*_{xz}, \tag{23}$$

$$\begin{aligned}-\frac{105\mathrm{Kn}}{32}\frac{P^*_{xz}\sqrt{T^*}}{p^*}\frac{dT^*}{d\xi}&=q^*_x+\frac{21}{10}\gamma q^*_z+\frac{15\mathrm{Kn}^2\mathcal{F}}{8}\sqrt{T^*}\\&\quad+\frac{21\mathrm{Kn}^2\mathcal{F}}{8}\frac{\sqrt{T^*}P^*_{xz}\gamma}{p^*}\\&\quad-\frac{15\mathrm{Kn}^2\mathcal{F}}{16}\frac{\sqrt{T^*}P^*_{zz}}{p^*},\end{aligned} \tag{24}$$

$$\begin{aligned}&-\frac{75\mathrm{Kn}}{32}\frac{\sqrt{T^*}P^*_{zz}}{p^*}\frac{dT^*}{d\xi}-\frac{9\mathrm{Kn}}{8}\frac{\sqrt{T^*}}{p^*}\frac{d}{d\xi}(\gamma T^*P^*_{xz})\\&=\frac{3}{5}\gamma q^*_x+q^*_z-\frac{15\mathrm{Kn}^2\mathcal{F}}{16}\frac{P^*_{xz}\sqrt{T^*}}{p^*},\end{aligned} \tag{25}$$

$$\frac{5\mathrm{Kn}}{16}\frac{\sqrt{T^*}}{p^*}\frac{dq^*_z}{d\xi}=-P^*_{xz}\gamma. \tag{26}$$

The other diagonal components of P^*_{ij} and the hydrostatic pressure are

$$P^*_{xx}=P^*_{zz}-\frac{14}{5}\gamma P^*_{xz},\quad P^*_{yy}=P^*_{zz}-\frac{4}{5}\gamma P^*_{xz},$$

$$p^*=P^*_{zz}-\frac{6}{5}\gamma P^*_{xz}. \tag{27}$$

The boundary conditions are $T^*(\pm\frac{1}{2})=1$. The fields T^*, P^*_{zz}, and q^*_z are even in $\mathcal{F}$ while P^*_{xz}, γ, and q^*_x are odd. The integral condition stemming from the equation of state is again $\int_{-1/2}^{1/2}(p^*/T^*)d\xi=1$.

The second-order solution to the above system of equations is

$$\begin{aligned}T^*&=1+\left(\left[\frac{14\xi^2}{25}-\frac{7}{50}\right]\mathrm{Kn}^2+\left[\frac{1133}{1125}-\frac{128\xi^4}{1125}\right]\right)\mathcal{F}^2,\\ \gamma&=-\mathrm{Kn}\mathcal{F}\xi,\\ P^*_{zz}&=1+\left(\frac{5657}{5625}-\frac{29\mathrm{Kn}^2}{150}\right)\mathcal{F}^2,\quad P^*_{xz}=\mathrm{Kn}\mathcal{F}\xi,\\ q^*_x&=-\frac{15\mathrm{Kn}^2\mathcal{F}}{16},\quad q^*_z=\frac{16\mathrm{Kn}\mathcal{F}^2\xi^3}{15}.\end{aligned} \tag{28}$$

The temperature at this order has a minimum at the center of the channel but it has symmetric maxima quite near the center, at $\xi\approx\pm 1.57\mathrm{Kn}$. After we made this observation we saw that a similar conclusion is made in [15,16].

In the following section we discuss some of the implications of these results.

V. DISCUSSION AND CONCLUSIONS

It has been shown that Boltzmann's equation implies a gas-dynamics that has a more complex nature than standard hydrodynamics. We stress again that no constitutive transport equations were assumed, but rather the theoretical framework itself gave us highly nonlinear equations that take the place of the usual Newton's and Fourier's transport laws.

Since we have dealt with a laminar stationary flow, it was possible to derive analytic perturbative expressions for every hydrodynamic field and compare them with what was measured in our simulations. The effects beyond standard hydrodynamics should be observable, and are correctly described with our expressions, within a small error margin, and they have obvious relevance in straightforward molecular dynamics.

Most of our work refers to the two-dimensional case since

this is the system that we are able to simulate. In fact, in spite of the efficiency of our simulator [21] and the quality of our computational equipment, we are not yet able to run the simulations as long as needed with a system of an equivalent size in three dimension (of at least $84^3=592\,704$ particles).

One can, however, discuss the implications of the results in three dimensions, given in Sec. IV, and argue that under appropriate conditions these effects can (hopefully) be observed in real experiments. It is easy to derive that the ratio between the velocity at the center of the channel $v_{\max}$ and the thermal velocity $v_{\rm th}=2\sqrt{2T_0/(\pi m)}$ is $v_{\max}/v_{\rm th}=\sqrt{\pi}\mathcal{F}/10$. Requiring that this ratio is less than 1.0 implies that $\mathcal{F}<5.64$. On the other hand, the Reynolds number defined as $\mathrm{Re}=v_{\max}L_z/\nu$, where ν is the ideal gas kinetic shear viscosity, turns out to be $\mathrm{Re}=16\mathcal{F}/(25\mathrm{Kn})$ and the ratio between the abnormal heat flux q_x and the transversal (normal) component q_z is $q_x/q_z=9/(2\mathrm{Re})$, telling us that to make the effects of q_x more evident we need a Reynolds number not too large.

To make a numerical estimate of what has been said, let us take $\mathrm{Kn}=1/(\sqrt{2\pi}n\sigma^2L_z)=0.06$, see Eq. (21), as the one used in our bidimensional simulations but considering a realistic value of the diameter for the particles $\sigma=10^{-10}$ (m). Requiring $L_z=1$ (m) the number density n turns out to be about $n_0/40$, where n_0 is the density obtained dividing the Avogadro number by 22.4 liters. If we further use the value $\mathcal{F}=2.0$, then near the walls $q_x/q_z\approx 0.2$, namely, the longitudinal heat flux component is 20% the value of the normal transversal component. For these values of the parameters one can also check that the second-order corrections to the hydrodynamic fields are quite appreciable, particularly those on the temperature and on P_{zz}.

ACKNOWLEDGMENTS

This work has been partially financed by Fondecyt Grant No. 197 0786, by Fundación Andes Grant No. C-12971, and by UBB Diprode research Grant No. 970905-2. We thank L. Letamendia for his hospitality at U. Bordeaux I and W. Ellison for his help in the use of the Cray belonging to the Laboratorie Physique des Interactions Ondes-Matière, ENSCPB, U. de Bordeaux I. This work was also supported by a ECOS-Conicyt grant.

APPENDIX: SOLUTION UP TO SIXTH ORDER IN $\mathcal{F}$ IN DIMENSION TWO

We have solved self-consistently the differential equations up to sixth order in $\mathcal{F}$ using MAPLE. It is possible to go further up, but this order seems more than enough for our present purposes.

$$\gamma=-\xi\mathcal{F}\mathrm{Kn}+\left(-\frac{79\xi^3\mathrm{Kn}^3}{24}+\frac{27\xi\mathrm{Kn}^5}{64}-\frac{3\xi\mathrm{Kn}^3}{16}+\frac{\xi\mathrm{Kn}}{48}-\frac{\xi^5\mathrm{Kn}}{15}\right)\mathcal{F}^3+\left(-\frac{101\xi^9\mathrm{Kn}}{5670}-\frac{237\xi^3\mathrm{Kn}^5}{128}-\frac{189\xi\mathrm{Kn}^9}{2048}+\frac{2687\xi^3\mathrm{Kn}^7}{384}\right.$$
$$\left.-\frac{3751\xi\mathrm{Kn}^5}{15360}-\frac{601\xi^7\mathrm{Kn}^3}{840}+\frac{351\xi\mathrm{Kn}^7}{1024}-\frac{1723\xi^5\mathrm{Kn}^5}{120}-\frac{7\xi^5\mathrm{Kn}^3}{240}+\frac{17\xi^5\mathrm{Kn}}{3600}+\frac{79\xi^3\mathrm{Kn}^3}{384}+\frac{77\xi\mathrm{Kn}^3}{5760}-\frac{137\xi\mathrm{Kn}}{161280}\right)\mathcal{F}^5, \tag{A1}$$

$$T^*=1+\left(-\frac{\xi^4}{3}-\frac{3\mathrm{Kn}^2}{16}+\frac{3\mathrm{Kn}^2\xi^2}{4}+\frac{1}{48}\right)\mathcal{F}^2+\left(-\frac{\mathrm{Kn}^2\xi^6}{45}-\frac{31\xi^8}{630}+\frac{29\mathrm{Kn}^4\xi^4}{12}+\frac{9\xi^2\mathrm{Kn}^4}{64}+\frac{27\mathrm{Kn}^6}{512}+\frac{\mathrm{Kn}^2}{180}-\frac{67}{161280}-\frac{143\mathrm{Kn}^4}{768}\right.$$
$$-\frac{\mathrm{Kn}^2\xi^2}{64}-\frac{\mathrm{Kn}^2\xi^4}{48}+\frac{7\xi^4}{720}-\frac{27\mathrm{Kn}^6\xi^2}{128}\Big)\mathcal{F}^4+\left(\frac{1157\xi^{10}\mathrm{Kn}^2}{113400}+\frac{29\mathrm{Kn}^2\xi^4}{10080}-\frac{1823\xi^{12}}{133650}-\frac{189\mathrm{Kn}^{10}}{16384}-\frac{189\mathrm{Kn}^8\xi^2}{1024}+\frac{189\mathrm{Kn}^{10}\xi^2}{4096}\right.$$
$$-\frac{31\mathrm{Kn}^2\xi^8}{2016}+\frac{63707\mathrm{Kn}^6\xi^6}{5760}-\frac{2141\mathrm{Kn}^4\xi^4}{11520}+\frac{128731\xi^8\mathrm{Kn}^4}{40320}+\frac{693\mathrm{Kn}^6\xi^4}{512}-\frac{7\,\xi^6\mathrm{Kn}^4}{720}-\frac{36413\mathrm{Kn}^2}{116121600}-\frac{77\xi^2\mathrm{Kn}^4}{7680}+\frac{3721\mathrm{Kn}^4}{2064384}$$
$$-\frac{22249\mathrm{Kn}^6}{73728}+\frac{17\mathrm{Kn}^2\xi^6}{10800}+\frac{1817\mathrm{Kn}^6\xi^2}{10240}+\frac{32837\mathrm{Kn}^8}{98304}+\frac{62437}{3832012800}+\frac{137\mathrm{Kn}^2\xi^2}{215040}+\frac{589\xi^8}{151200}-\frac{9817\xi^4}{21772800}$$
$$\left.-\frac{28301\mathrm{Kn}^8\xi^4}{6144}\right)\mathcal{F}^6, \tag{A2}$$

$$q_x^*=-\mathcal{F}\mathrm{Kn}^2+\left(\frac{73\mathrm{Kn}^2\xi^4}{6}-\frac{27\xi^2\mathrm{Kn}^4}{8}+\frac{3\mathrm{Kn}^4}{32}-\frac{\mathrm{Kn}^2}{96}\right)\mathcal{F}^3+\left(-\frac{243\mathrm{Kn}^6\xi^2}{256}-\frac{173\mathrm{Kn}^4}{46080}+\frac{599\mathrm{Kn}^6}{6144}+\frac{169\mathrm{Kn}^2}{645120}+\frac{27\xi^2\mathrm{Kn}^4}{256}\right.$$
$$\left.-\frac{1387\mathrm{Kn}^2\xi^4}{2880}+\frac{365\xi^4\mathrm{Kn}^4}{192}-\frac{11261\mathrm{Kn}^6\xi^4}{384}+\frac{6001\mathrm{Kn}^2\xi^8}{2520}+\frac{33107\xi^6\mathrm{Kn}^4}{720}+\frac{189\mathrm{Kn}^8\xi^2}{256}-\frac{27\mathrm{Kn}^8}{1024}\right)\mathcal{F}^5, \tag{A3}$$

$$q_y^*=\frac{8}{3}\xi^3\mathcal{F}^2\mathrm{Kn}+\left(\frac{12\xi^7\mathrm{Kn}}{35}+\frac{112\xi^5\mathrm{Kn}^3}{15}-\frac{\xi^3\mathrm{Kn}^3}{12}-\frac{\xi^3\mathrm{Kn}}{20}-\frac{9\xi^3\mathrm{Kn}^5}{8}\right)\mathcal{F}^4+\left(\frac{14579\xi^{11}\mathrm{Kn}}{155925}+\frac{719\xi^9\mathrm{Kn}^3}{405}+\frac{3\xi^7\mathrm{Kn}^3}{40}+\frac{4471\xi^7\mathrm{Kn}^5}{168}\right.$$
$$\left.-\frac{33\xi^7\mathrm{Kn}}{1400}-\frac{2533\xi^5\mathrm{Kn}^7}{192}+\frac{77\xi^5\mathrm{Kn}^5}{30}-\frac{203\xi^5\mathrm{Kn}^3}{450}-\frac{105\xi^3\mathrm{Kn}^7}{256}-\frac{481\xi^3\mathrm{Kn}^3}{120960}+\frac{59\xi^3\mathrm{Kn}^5}{960}+\frac{22843\xi^3\mathrm{Kn}}{10886400}+\frac{63\xi^3\mathrm{Kn}^9}{256}\right)\mathcal{F}^6, \tag{A4}$$

$$P_{xy}^{*}=\xi\mathcal{F}\mathrm{Kn}+\left(-\frac{\xi\mathrm{Kn}^3}{16}-\frac{\xi\mathrm{Kn}}{240}+\frac{\xi^3\mathrm{Kn}^3}{4}+\frac{\xi^5\mathrm{Kn}}{15}\right)\mathcal{F}^3+\left(\frac{\xi^5\mathrm{Kn}^3}{80}+\frac{5\xi^3\mathrm{Kn}^5}{64}+\frac{2\xi^7\mathrm{Kn}^3}{63}-\frac{13\xi^5\mathrm{Kn}}{3600}-\frac{11\xi^3\mathrm{Kn}^3}{960}+\frac{7\xi^5\mathrm{Kn}^5}{15}+\frac{101\xi^9\mathrm{Kn}}{5670}+\frac{1133\xi\mathrm{Kn}}{7257600}+\frac{\xi\mathrm{Kn}^3}{630}-\frac{187\xi\mathrm{Kn}^5}{3840}+\frac{9\xi\mathrm{Kn}^7}{256}-\frac{9\xi^3\mathrm{Kn}^7}{64}\right)\mathcal{F}^5, \tag{A5}$$

$$P_{xx}^{*}=1+\left(-\frac{\mathrm{Kn}^2}{4}+\frac{1}{60}+3\mathrm{Kn}^2\xi^2\right)\mathcal{F}^2+\left(\frac{45\mathrm{Kn}^6}{512}-\frac{157}{453600}+\frac{89\mathrm{Kn}^2}{13440}-\frac{857\mathrm{Kn}^4}{3840}+\frac{2\mathrm{Kn}^2\xi^6}{5}+\frac{85\mathrm{Kn}^4\xi^4}{8}+\frac{3\mathrm{Kn}^4\xi^2}{8}-\frac{3\mathrm{Kn}^2\xi^2}{40}-\frac{81\xi^2\mathrm{Kn}^6}{64}\right)\mathcal{F}^4+\left(\frac{991\mathrm{Kn}^2\xi^2}{302400}-\frac{8557\mathrm{Kn}^6}{24576}-\frac{54841\mathrm{Kn}^2}{159667200}+\frac{3\mathrm{Kn}^4\xi^6}{20}+\frac{568\mathrm{Kn}^2\xi^{10}}{4725}-\frac{17\mathrm{Kn}^4\xi^4}{24}+\frac{567\mathrm{Kn}^{10}\xi^2}{2048}-\frac{315\mathrm{Kn}^{10}}{163\ 84}+\frac{2999\mathrm{Kn}^6\xi^6}{64}-\frac{3\mathrm{Kn}^2\xi^6}{100}+\frac{26383\mathrm{Kn}^8}{61440}+\frac{282839\mathrm{Kn}^4}{58060800}+\frac{53441}{3891888000}-\frac{227\mathrm{Kn}^4\xi^2}{6720}+\frac{59\mathrm{Kn}^4\xi^8}{20}+\frac{85\mathrm{Kn}^6\xi^4}{16}-\frac{27\mathrm{Kn}^8\xi^2}{32}-\frac{5563\mathrm{Kn}^8\xi^4}{256}+\frac{285\xi^2\mathrm{Kn}^6}{512}\right)\mathcal{F}^6, \tag{A6}$$

$$P_{yy}^{*}=1+\left(-\frac{\mathrm{Kn}^2}{4}+\frac{1}{60}\right)\mathcal{F}^2+\left(\frac{45\mathrm{Kn}^6}{512}-\frac{157}{453600}+\frac{89\mathrm{Kn}^2}{13440}-\frac{857\mathrm{Kn}^4}{3840}\right)\mathcal{F}^4\left(\frac{26383\mathrm{Kn}^8}{61440}-\frac{8557\mathrm{Kn}^6}{24576}+\frac{53441}{3891888000}+\frac{282839\mathrm{Kn}^4}{58060800}-\frac{315\mathrm{Kn}^{10}}{16384}-\frac{54841\mathrm{Kn}^2}{159667200}\right)\mathcal{F}^6. \tag{A7}$$

[1] L. D. Landau and L. M. Lifschitz, *Fluid Mechanics* (Pergamon Press, Oxford, 1959).

[2] S. A. Orzag and L. C. Kells, J. Fluid Mech. **96**, 159 (1980).

[3] *Hydrodynamic Instability and the Transition to Turbulence*, edited by H. L. Swinney and J. P. Gollub (Springer Verlag, Berlin, 1985).

[4] L. Hanon, G. C. Lie, and E. Clementi, Phys. Lett. A **119**, 174 (1986).

[5] M. Alaoui and A. Santos, Phys. Fluids A **4**, 1273 (1992).

[6] L. P. Kadanoff, G. R. McNamara, and G. Zanetti, Phys. Rev. A **40**, 4527 (1989).

[7] J. Koplik, J. R. Banavar, and J. F. Willemsem, Phys. Rev. Lett. **60**, 1282 (1988).

[8] A. Fortin, M. Jardak, J. J. Gervais, and R. Pierre, J. Comput. Phys. **115**, 455 (1994).

[9] H. Grad, Commun. Pure Appl. Math. **2**, 331 (1949); H. Grad, *Principle of the Kinetic Theory of Gases*, in *Handbuch der Physik, Vol. XII*, edited by S. Flüge (Springer, Berlin, 1958).

[10] D. Risso and P. Cordero, Phys. Rev. E **56**, 489 (1997); **57**, 7364 (E) (1998).

[11] P. Cordero and D. Risso, in *Fourth Granada Lectures in Computational Physics*, edited by P. L. Garrido and J. Marro (Springer-Verlag, Berlin, 1997).

[12] P. Cordero and D. Risso, Physica A (to be published).

[13] J. H. Ferziger and H. G. Kaper, *Mathematical Theory of Transport Processes in Gases* (North-Holland, Amsterdam, 1972).

[14] M. Tij and A. Santos, J. Stat. Phys. **76**, 1399 (1994).

[15] M. Tij, M. Sabbane, and A. Santos, Phys. Fluids **10**, 1021 (1998).

[16] M. Malek Mansour, F. Baras, and Alejandro L. Garcia, Physica A **240**, 255 (1997).

[17] J. M. Montanero and V. Garzó, Phys. Rev. E (to be published).

[18] A. Baranyai, D. J. Evans, and P. J. Daivis, Phys. Rev. A **46**, 7543 (1992).

[19] B. D. Todd and D. J. Evans, Phys. Rev. E **22**, 2800 (1997).

[20] D. Henderson, Mol. Phys. **30**, 971 (1975).

[21] M. Marín, D. Risso, and P. Cordero, J. Comput. Phys. **109**, 306 (1993).